Heliyon 10 (2024) e32889

Contents lists available at ScienceDirect

Heliyon

journal homepage: www.cell.com/heliyon

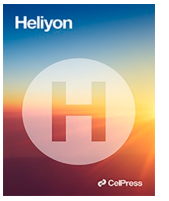

Research article

HIF-1α activation impairs dendrites formation and elongation in osteocytogenesis

Xiaoyan Li [a,b,1], Jian Zhao [c,1], Lei Chen [b,1], Xinyi Zhou [d], Minglong Qiu [d], Lianfu Deng [d,**], Kai Yang [d,***], Yaozeng Xu [a,*]

[a] Department of Orthopaedics, The First Affiliated Hospital of Soochow University, No. 188 Shizi Street, Suzhou, Jiangsu, 215006, China
[b] Department of Orthopaedics, Affiliated Hospital of Jining Medical University, No. 89, Guhuai Road, Jining, 272029, Shandong Province, China
[c] Department of Orthopaedics, The Affiliated Taian City Central Hospital of Qingdao University, Taian, 271000, Shandong, China
[d] Department of Orthopaedics, Shanghai Key Laboratory for Prevention and Treatment of Bone and Joint Diseases, Shanghai Institute of Traumatology and Orthopaedics, Ruijin Hospital, Shanghai Jiao Tong University School of Medicine, 197 Ruijin 2nd Road, Shanghai, 200025, China

ARTICLE INFO

Keywords:
Osteocytogenesis
HIF
E11
RhoA
Bone homeostasis

ABSTRACT

Osteocytes are terminally differentiated cells derived from osteoblasts and are deeply embedded within the bone matrix. They play a critical role in bone remodeling by generating a lacuno-canalicular network (LCN) and controlling the transport of nutrients. Due to the absence of blood vessels within the bone matrix, it is widely believed that osteocytes develop in a hypoxic environment. However, the mechanisms of osteocytogenesis and the role of oxygen sensing in this process remain unclear. Hypoxia-inducible factors (HIFs) are major transcriptional factors involved in oxygen sensing. Previous studies have shown that accumulation of HIFs in osteoblasts leads to abnormal bone remodeling, potentially linked with the alterations of the LCN network. Specifically, HIF-1α is hypothesized to play a more significant role in regulating bone remodeling compared to HIF-2α. Therefore, we investigated the functions of HIF-1α in dendrite formation and the establishment of the LCN network during osteocytogenesis. Immunostaining and scanning electron microscopy revealed that the E11 protein aggregates to form a ring structure that defines the site for dendrite initiation. This process is followed by activation of the ERM/RhoA pathway and recruitment of matrix metalloproteinase 14 (MMP14) to facilitate extracellular matrix degradation, enabling dendrite elongation. However, both hypoxic treatment and overexpression of HIF-1α impair ring formation, resulting in reduced ERM/RhoA activity and decreased matrix degradation capability. These findings suggest that abnormal HIF-1α activity in local areas could contribute to impaired LCN network formation and abnormal bone remodeling observed in bone diseases such as osteopenia and aging.

* Corresponding author.
** Corresponding author. Shanghai Key Laboratory for Prevention and Treatment of Bone and Joint Diseases with Integrated Chinese-Western Medicine, Shanghai Institute of Traumatology and Orthopedics, Ruijin Hospital, Shanghai Jiao Tong University School of Medicine, 197 Ruijin 2nd Road, Shanghai, 200025, China.
*** Corresponding author. Shanghai Key Laboratory for Prevention and Treatment of Bone and Joint Diseases with Integrated Chinese-Western Medicine, Shanghai Institute of Traumatology and Orthopedics, Ruijin Hospital, Shanghai Jiao Tong University School of Medicine, 197 Ruijin 2nd Road, Shanghai, 200025, China.
E-mail addresses: lf_deng@126.com (L. Deng), cyan.kai@gmail.com (K. Yang), xuyaozeng@suda.edu.cn (Y. Xu).
[1] These authors contributed equally to this work.

https://doi.org/10.1016/j.heliyon.2024.e32889
Received 24 November 2023; Received in revised form 11 June 2024; Accepted 11 June 2024
Available online 17 June 2024

1. Introduction

At the final stage of bone formation, osteoblasts may enter a dormant state as bone lining cells, or undergo programmed cell death, or become deeply embedded in osteoid, where they differentiate into osteocytes [1,2]. Osteocytes inhabit bone lacunae, exhibiting a specialized morphology characterized by numerous cellular dendrites that connect with adjacent cells, forming an extensive cell-cell

Abbreviations

LCN	lacuno-canalicular network
VHL	von Hippel-Lindau
HIF	Hypoxia-inducible factor
OC	osteocalcin
DMP1	dentin matrix protein 1
MMP14	matrix metalloproteinase 14
SEM	scanning electron microscope
IF	immunofluorescence

network known as the lacuno-canalicular network (LCN) [3]. Through the LCN network, osteocytes play a pivotal role in maintaining bone homeostasis by secreting the osteoblastic inhibitor Sclerostin and the osteoclastic activator RANKL, in addition to regulating mineral and glucose homeostasis [4].

The LCN network facilitates the transport of nutrients and integrates biochemical and hormonal signals between osteocytes and other bone tissue cells [5]. Imaging studies in both human and animal models have revealed disorganized osteocyte networks in several bone diseases such as osteopenia and osteoarthritis [6]. Moreover, age-related changes are associated with decreased lacunae density and dysregulated LCN network organization [7], underscoring the critical role of the LCN network in skeletal homeostasis.

Due to the absence of blood vessels within the bone matrix, osteocytogenesis is thought to occur in a hypoxic environment [8]. Hypoxia-inducible factor (HIF)α serves as a major oxygen-sensing transcription factor, with three members in the HIFα protein family: HIF-1α, HIF-2α, and HIF-3α [9]. Under normal conditions, HIFα subunits undergo proline hydroxylation by proline hydroxylase domain proteins (PHDs) and subsequent ubiquitination by the E3 ligase complex VHL for degradation via the 26 S proteasome. However, under hypoxic conditions, prolyl hydroxylation of HIFα is inhibited, leading to its accumulation, translocation into the nucleus, and binding to HIF-β subunits to transactivate downstream genes [10].

Previous findings from our research group revealed impaired LCN networks and abnormal skeletal homeostasis in osteocalcin (OC)

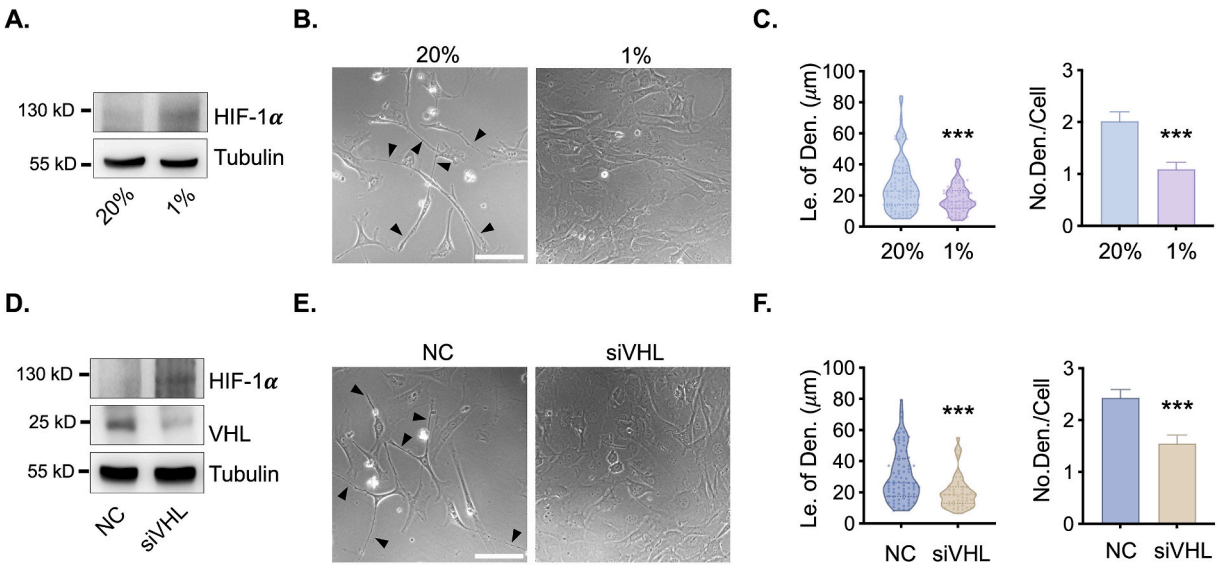

Fig. 1. Hypoxic environment inhibits dendrites formation in preosteocytes. (**A, D**) The HIF-1α protein level in IDG-SW3 cells under hypoxia treatment (1 % O_2) for 24 h (**A**) or after VHL siRNA knockdown after 48 h (**D**). (**B, E**) Representative images of dendrites under hypoxia treatment (**B**) or after VHL siRNA knockdown in IDG-SW3 cells (**E**). (**C, F**) Statistical analysis of the dendrite's length (Le. of Den., $n = 50–95$ dendrites) and number of dendrites per cell (No.Den./Cell, $n = 40–55$ cells) in **B** or **E**. Data was shown as mean ± S.E.M. Triplicated experiments were performed and representative data was shown. ***, $p < 0.01$. Uncropped images in A and **D** are available in Supplementary Fig. S1. Raw data is available in Table 1.

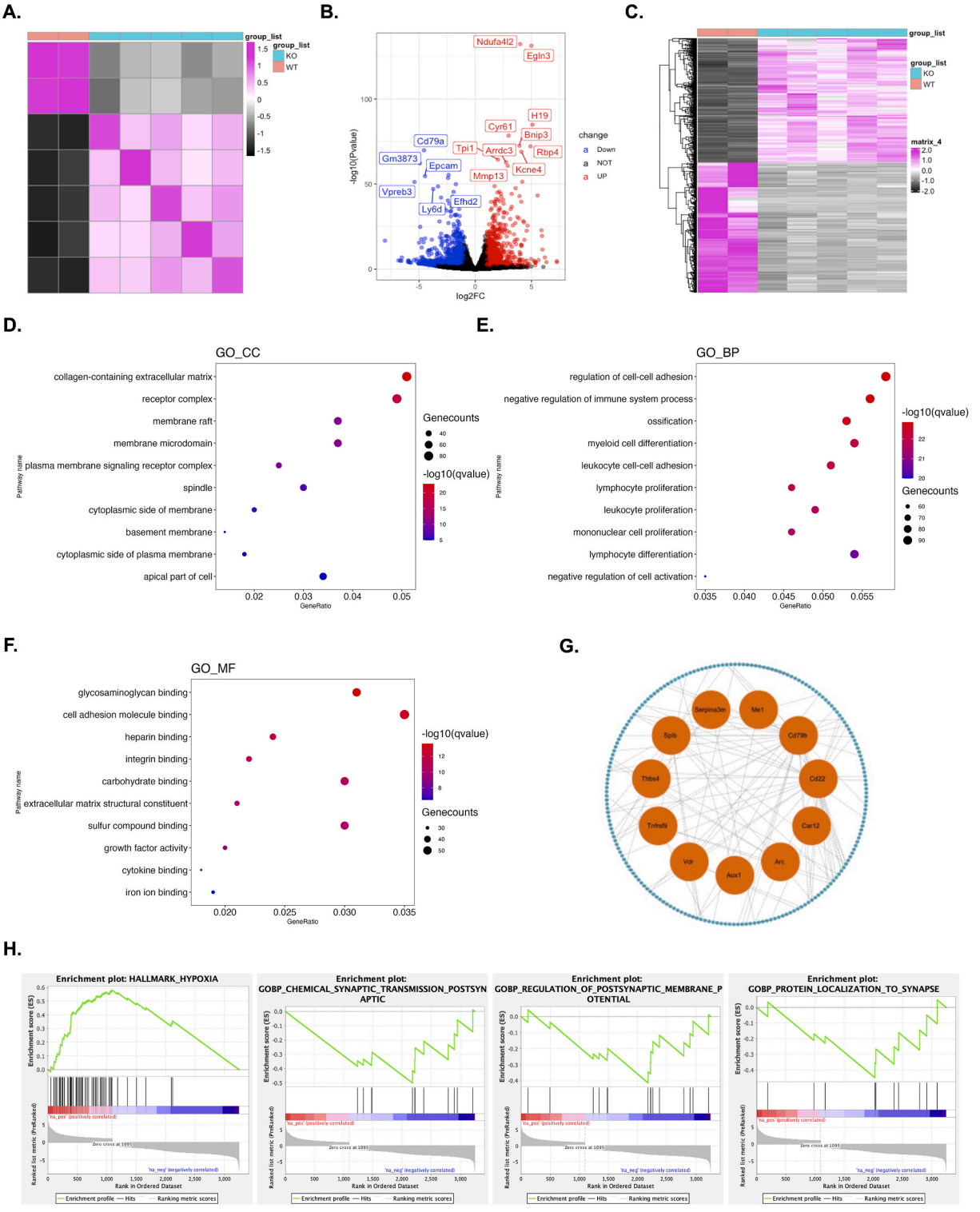

Fig. 2. Impact of VHL absence on membrane movement and cytoskeleton dynamics. (**A**) Heatmap of osteocyte transcriptomes from WT (n = 2) and VHL^{OC} mice (n = 5). (**B**) Volcano plot of differentially expressed genes between WT and VHL^{OC} mice. (**C**) Heatmap of DEGs between WT and VHL^{OC} mice. (**D to F**) Bubble plots showing Gene Ontology (GO) analysis results of DEGs in WT and VHL^{OC} mice. BP: Biological Process (**D**), CC: Cellular Component (**E**), MF: Molecular Function (**F**). (**G**) Protein-Protein Interaction (PPI) network of cell membrane-associated DEGs with other DEGs. (**H**) Gene set enrichment analysis (GSEA) analysis of HALLMARK and GOBP between WT and VHL^{OC} mice. Original data is available in Table 1.

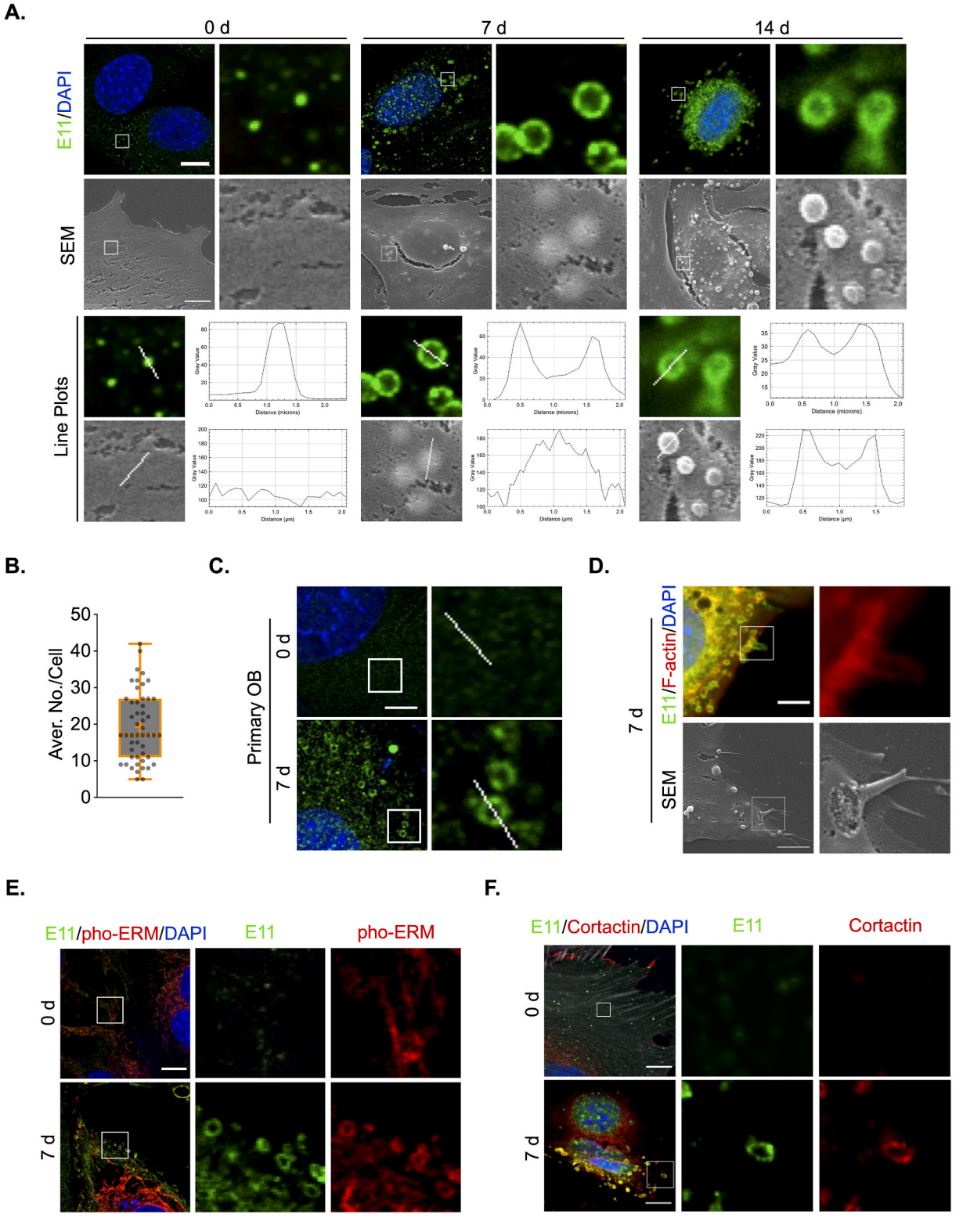

(caption on next page)

Fig. 3. E11 forms a ring structure to define dendrite formation sites. (**A**) Endogenous E11 IF (upper) and SEM images (middle) of IDG-SW3 cells cultured in osteogenic medium at indicated time. Line profiles (bottom) of ring structure in IF and SEM images. (**B**) Statistical analysis of the number of E11 positive ring structures per cell in **A**. $n = 50$ cells. Data was shown as box plot with min to max value. (**C**) Representative endogenous E11 localization images of primary osteoblasts cultured in osteogenic medium at indicated time. (**D to F**) Representative endogenous E11 IF images co-stained with F-actin (**D**), pho-ERM (**E**) and Cortactin (**F**) in IDG-SW3 cells cultured in osteogenic medium at indicated time. F-actin was stained with Texas Red-X conjugated phalloidin. Nucleus were counterstained with DAPI. Triplicated experiments were performed and representative data was shown. Scale bars, **A**, 10 μm, **C, D,** 5 μm, **E, F,** 10 μm d, day. Raw data is available in Table 1.

and dentin matrix protein 1 (DMP1) derived VHL conditional knockout mice [9,11]. Studies by Shomento et al. demonstrated that mice lacking HIF-1α, but not HIF-2α, exhibit marked impairment in bone remodeling, implicating the regulatory role of HIF-1α in the LCN network. However, the specific mechanisms remain unclear.

In this study, we demonstrate that HIF signaling regulates LCN homeostasis by modulating dendrite formation and elongation during osteocytogenesis. We observed that E11 protein aggregates to form a ring structure defining the dendrite initiation site. Subsequent activation of the ERM/RhoA pathway after E11 aggregation recruits matrix metalloproteinase 14 (MMP14) to degrade the extracellular matrix and promote dendrite elongation. However, hypoxic treatment and HIF-1α overexpression reduce the number of ring structures, along with the activity of the ERM/RhoA pathway and matrix degradation. Therefore, the impaired LCN network in VHL mutant mice is partially attributed to impaired E11-ERM-RhoA activity resulting from HIF-1α activation. These findings shed light on the role of HIF-1α in regulating osteocytogenesis and bone homeostasis.

2. Results

2.1. Hypoxic environment inhibits dendrites formation in preosteocytes

To mimic the hypoxic conditions found in bone tissue where osteocytes reside, we subjected cells to hypoxia treatment (1 % O_2) for 24 h and employed VHL siRNA knockdown for 48 h to activate the HIF pathway. The results demonstrated a marked accumulation of HIF-1α protein under hypoxic conditions compared to the normal state (20 % O_2) (Fig. 1A). Additionally, bright-field microscopy revealed a reduction in the dendrite network (Fig. 1B). Statistical analysis indicated a decrease in both the length (Len. of Den.) and number of dendrites per cell (No.Den./Cell) after hypoxic treatment (Fig. 1C, and Table 1). Similarly, VHL knockdown via siRNA yielded comparable results (Fig. 1D–F, Table 1). Thus, the hypoxic environment diminishes dendrite formation in preosteocytes.

2.2. Impact of VHL absence on membrane movement and cytoskeleton dynamics

To investigate the pathways influenced by VHL depletion and their association with dendrite formation, osteocytes from VHL^{OC} mice (n = 5) and littermate control mice (n = 2) were isolated separately and subjected to bulk RNA-seq sequencing. Principal component analysis (PCA) revealed that the gene expression profile of VHL^{OC} mice was consistent within the group but significantly differed from that of control mice (Fig. 2A). Applying a threshold of $|Log2FC| > 1$ & PValue <0.01, we identified a total of 2118 differentially expressed genes (DEGs), comprising 888 upregulated and 1230 downregulated genes, from the combined dataset using the *EdgeR* package for analysis in *R*, as depicted in volcano and heatmap plots (Fig. 2B and C, and Table 1).

To explore the potential biological changes of these screened DEGs, GO enrichment analysis were performed using the DAVID online database and exported into the *R* environment for visualization. The GO_CC (cellular component) results showed that the DEGs were mainly enriched in extracellular matrix, receptor complex, membrane raft, membrane microdomain, and plasma membrane signaling receptor complex. Most of the Top 10 GO_CC pathways were enriched in membrane-related component (Fig. 2D, and Table 1). The results of GO_BP (biological process) annotation showed that the DEGs were mainly enriched in cell-cell adhesion, ossification and cell differentiation (Fig. 2E, and Table 1). GO_MF (molecular function) enrichment annotation showed that the DEGs were mainly enriched in membrane molecule binding (Fig. 2F, and Table 1). Using Cytoscape's internal analysis plug-in, *MCODE*, the PPI network of DEGs was filtered to gain the subnetworks with the highest clustering scores for visualizing (Fig. 2G). As shown in the figure, we hypothesized that *Me1*, *Cd22*, *Cd79b*, *Car12*, *Vdr*, *Aox1*, *Thbs4* and *Tnfrsf9* are hub genes, which were both enriched in synapse initiation event.

Furthermore, the DEGs were subjected to the GSEA enrichment analysis to explore weighted changes. Using the gene set *msigdb.v2023.1.Mm.symbols* for GSEA analysis and excluding results without statistical significance, we found that synapse-related pathways were significantly inhibited in VHL-depleted osteoblasts (Fig. 2H), consistent with the reduced lacuno-canalicular network observed in VHL^{OC} mice.

2.3. E11 forms a ring structure to define dendrite formation sites

Dendrite formation and elongation during osteocytogenesis are closely associated with the transmembrane glycoprotein E11, widely expressed in various body tissues [12]. However, the membranal localization of E11 during osteocytogenesis has not been visualized. Therefore, IDG-SW3 cells were cultured in osteogenic medium for 14 days, and the dynamic changes in the position of E11 protein during osteocytogenesis were analyzed using immunofluorescence (IF) staining techniques. Representative images demonstrated that scattered E11 dots in undifferentiated IDG-SW3 cells aggregated into a ring structure by Day 7, and enhanced by Day 14 (Fig. 3A, upper).

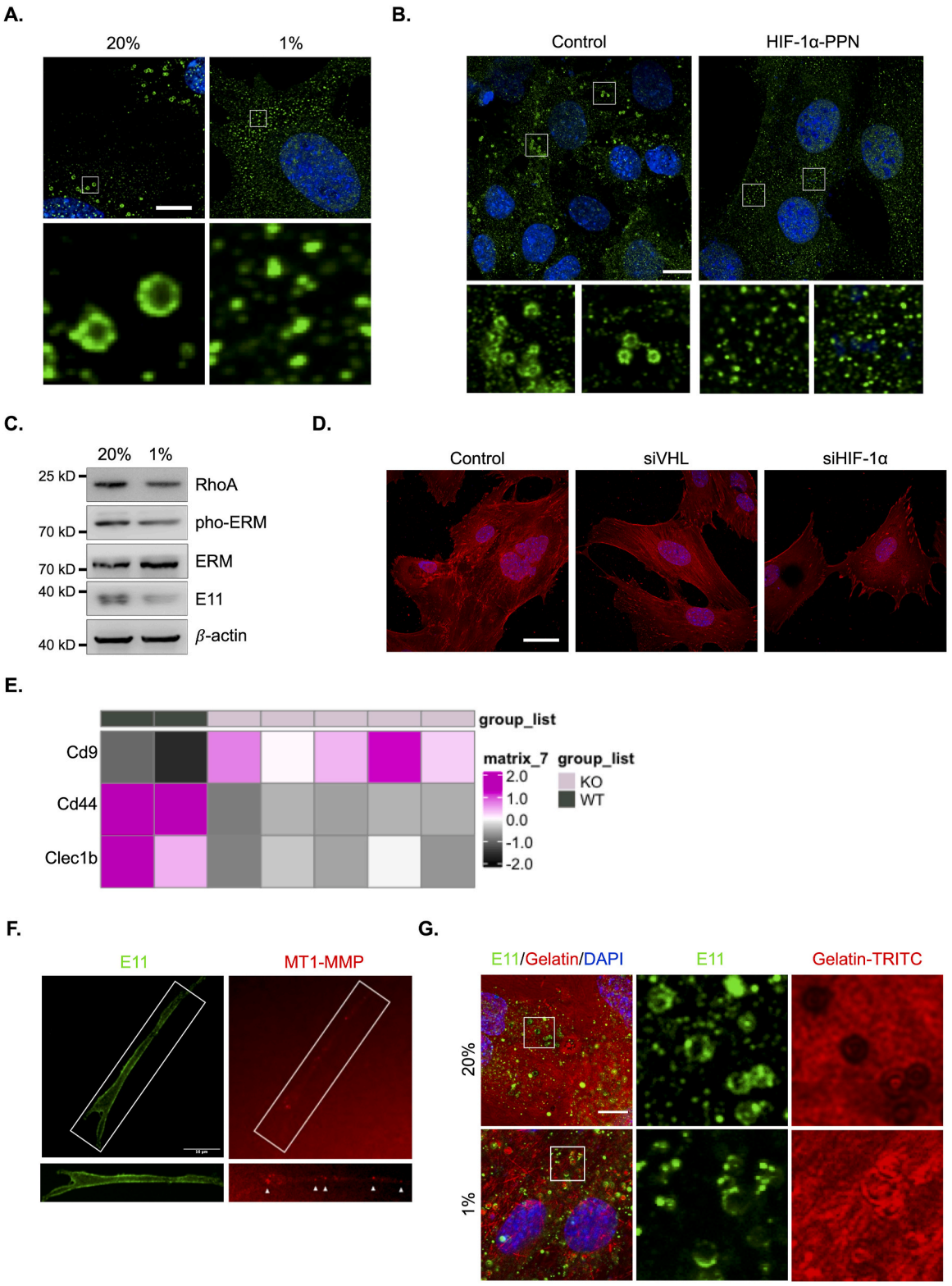

Fig. 4. Hypoxic environment and HIF-1α overexpression inhibit dendrite formation and matrix degradation. (**A, B**) Endogenous E11 IF in hypoxia treated (1 % O_2) IDG-SW3 cells (**A**) or in HIF-1α-PPN transfected IDG-SW3 cells (**B**). (**C**) Protein level of RhoA, phosphorylated ERM, total ERM, E11 and *β*-actin were analyzed by Western blot. (**D**) Representative cytoskeleton images in VHL and HIF-1α siRNA knock down IDG-SW3 cells, stained with Texas Red-X conjugated phalloidin. (**E**) Relative value of *Cd9*, *Cd44*, *Clec1b* mRNA level between WT ($n = 2$) and VHL^{OC} mice ($n = 5$),

analyzed by RNA-seq. (**F**) Representative images of dendrite from osteogenic cultured IDG-SW3 cells, co-stained with MT1-MMP and E11. MT1-MMP positive vesicles are indicated with white arrows. (**G**) Gelatin-degradation assay of osteogenic cultured IDG-SW3 cells on glass coverslips coated with FITC-crosslinked gelatin, after culturing in normal (20 % O_2) or hypoxia (1 % O_2) conditions for 24 h. Triplicated experiments were performed and representative data was shown. Scale bars, **A**, **B**, **F**, **G**, 10 μm, **D**, 20 μm, magnification scale bars, **F**, 5 μm, **A**, **B**, **G**, 2 μm. Nucleus were counterstained with DAPI. Uncropped images are available in Supplementary Fig. S1. Raw data is available in Table 1.

Furthermore, scanning electron microscope (SEM) images revealed several protrusions formed on the cell membrane by Day 7, becoming more pronounced by Day 14, a phenomenon absents in undifferentiated cells at Day 0 (Fig. 3A, middle). Line profile analysis revealed that the average diameter of the rings in IF images and the protrusions in SEM images were comparable, ranging from 0.5 μm to 1 μm (Fig. 3A, bottom, line plots), suggesting these structures might be relative membranal structures during osteocytogenesis. Additionally, the number of ring structures per cell was calculated, varying from 10 to 40 per cell (Fig. 3B, and Table 1), consistent with the reported number of 50 dendrites per osteocyte in cortical bone [6].

To confirm whether this phenomenon is a universal mechanism during osteocytogenesis, primary osteoblasts derived from calvarias were isolated and subjected to IF experiments against E11. Consistent with previous data, E11 protein in osteogenic differentiated primary osteoblasts (OB) also formed a ring structure (1 μm) on the membrane by Day 7 (Fig. 3C).

Moreover, to confirm that this structure is an actin-rich cell membrane, the localization of F-actin, phosphorylated ERM, and Cortactin, involved in cytoskeleton dynamics and contraction, were visualized during osteocytogenesis. Representative images indicated that the E11 formed ring structure rich in F-actin, phosphorylated ERM, and Cortactin (Fig. 3D–F). Importantly, SEM images in Fig. 3D revealed a dendrite sprouting from the cell membrane over the flattened filopodia.

These pieces of evidence strengthen the notion that the E11 ring structure defines sites for dendrite generation and recruits cytoskeletal proteins to promote dendrite formation and extension.

2.4. Hypoxic environment and HIF-1α overexpression inhibit dendrite formation and matrix degradation

We investigated the mechanisms underlying dendrite inhibition in a hypoxic environment. Hypoxia treatment (1 % O_2) for 24 h resulted in the significant disappearance of already formed E11 ring structures in differentiated IDG-SW3 cells by Day 6 (Fig. 4A). Given that HIF-2α protein functions in promoting chondrogenesis and no apparent abnormalities in the LCN network were observed in HIF-2α constitutively activated mice, we postulated that the abnormal LCN network in VHL^{OC} mice is primarily attributed to HIF-1α activation [13]. Therefore, a PHD resistant HIF-1α mutation vector, with three mutation sites in the ODD region (Pro402, Pro564) and the TAD region (Asn803) (referred to as HIF-1α-PPN) [14], was transfected into IDG-SW3 cell at Day 0, and subjected to osteogenic differentiation until Day 7. Representative images revealed that the formation of the E11 ring structure in the HIF-1α-PPN group was markedly abolished (Fig. 4B). To further confirm the status of the E11 pathway, we assessed the expression of E11 and phosphorylation of ERM in HIF-1α-PPN-overexpressing cells. The results indicated reduced expression of E11 and phosphorylated ERM after HIF-1α-PPN overexpression (Fig. 4C).

According to literature, RhoA GTP enzyme, as one of the downstream effectors of ERM kinase, regulates stress fiber and focal adhesion formation [15]. Consistent with the reduction of RhoA expression in HIF-1α-PPN overexpressed-cells (Fig. 4C), the number of stress fibers were increased, and the number of focal adhesions were decreased after VHL known down with siVHL (Fig. 4D). *Vice versa*, HIF-1α siRNA knockdown increased the focal adhesions number, and reduces the number of stress fibers (Fig. 4D). These results revealed entire E11-ERM-RhoA signaling pathway is inhibited after HIF-1α activation.

Previous studies have reported that osteoblasts preparing to transform into osteocytes require cell-cell interaction with mature osteocytes to initiate osteocytogenesis [16]. interactions between surface molecules CD44 or Clec2 proteins with E11 promote cytoskeleton movement and directional migration, while CD9 molecules play a competitive negative regulatory role in their binding [17]. Therefore, we analyzed the mRNA levels of *Cd9*, *Cd44*, and *Clec1b* in VHL^{OC} mice using RNA-seq data. The heatmap revealed a significant decrease in *Cd44* and *Clec1b* gene transcription in mature osteocytes from VHL^{OC} mice, while *Cd9* expression increased (Fig. 4E, and Table 1). This indicates that inactivation of the E11-ERM-RhoA signaling axis is partly attributed to reduced receptor complex expression after HIF pathway activation, consistent with GO_CC pathways enrichment results (Fig. 2D).

During LCN network establishment, the elongation of osteocyte processes depends heavily on continuous degradation of type I collagen-enriched osteoid, primarily executed by MMP14. *Null* of *Mmp14* leads to disruption of collagen cleavage in osteocytes and abolished LCN network [17]. Initially, we used a gelatin matrix-contained 3D culture system to investigate MMP14 localization in osteogenic differentiated IDG-SW3 cells at Day 7 [18]. Representative images showed MMP14 protein aggregation in an already formed $E11^{+}$ dendrite (Fig. 4F).

Additionally, TRITC-gelatin-degradation assays were employed to detect whether the matrix degradation capability of already formed dendrites could be affected under hypoxic conditions. Osteogenic cultured IDG-SW3 cells at Day 7, considered preosteocytes, were seeded on TRITC-gelatin-coated coverslips and continuously cultured for 24 h. Representative images revealed that under normal conditions, the matrix area where E11 ring structures were located was degraded and turned into dark holes (Fig. 4G, upper). Conversely, hypoxic treatment completely disrupted matrix degradation (Fig. 4G, bottom).

In summary, we propose that HIF-1α activation not only inhibits dendrite formation but also suppresses their matrix degradation capability.

3. Discussion

Osteocytogenesis initiates with the embedding of mature osteoblasts into the osteoid [19]. Dendrites formation is considered as the typical morphological change at initiation stage. Although several related growth factors involved in this process have been discovered, yet the precise mechanisms driving this process remain elusive.

Proteomic studies by Tanaka and Kamioka et al. highlighted the heightened activity of cytoskeleton-related proteins in osteocytes, emphasizing the importance of cytoskeletal dynamics in osteocytogenesis, including membrane congestion and cell process extension. Our RNA-seq results corroborate this, indicating downregulation of cytoskeleton-related proteins in VHL^{OC} mice. Hence, impaired osteocyte maturation in VHL^{OC} mice may be linked to inactive cytoskeleton dynamics.

E11, a type I transmembrane mucin, is widely expressed in various tissues, including lymphatic endothelial cells, renal podocytes, tumor cells, osteoblasts and osteocytes [20–22]. In squamous carcinoma cells, E11 facilitates invasive capability via invadopodia-mediated matrix degradation [15]. E11's association with the ERM (Ezrin/radixin/moesin)-RhoA signaling cascade regulates actin cytoskeletal dynamics and cell shape remodeling [15,23,24]. Our study visualized E11 protein localization during osteocytogenesis, based on IDG-SW3 cells and primary osteoblasts revealing the formation of a ring structure on the membrane, akin to invadopodia's adhesion ring. However, the different thing is that, the E11 formed ring structures in preosteocytes are rounder, thicker (0.5–1 μm) and rarer (average 30 per cell), compare with the parameters of invadopodia in SCCs [15]. Thus, the dendrite in preosteocyte belongs to a tissue specific structure formed by E11 protein. Moreover, the cytoskeletal proteins, including Cortactin/MT1-MMP/Ezrin/F-actin, are both recruited to $E11^{+}$ adhesion rings in invadopodia [25,26], which is different with the osteocytic dendrites. Therefore, differences in structure and recruited cytoskeletal proteins suggest that dendrites and invadopodia are distinct subcellular structures, necessitating further investigation into dendrite formation mechanisms.

Numerous studies have implicated E11 in promoting dendrite formation and elongation [21,27,28]. We assumed that its activity potentially controlled by HIF-1α activation. We observed decreased activation levels of ERM and RhoA alongside downregulated E11 receptors, such as CD44 and Clec2, suggesting that reduced intercellular contact contributes to E11 downregulation. Interestingly, HIF-1α activation inhibited RhoA activity and local adhesion, contrasting with its role in breast cancer cells, where it enhances aggressive migration [29].

MMP14-mediated extracellular matrix degradation facilitates dendrite elongation and LCN network formation [30]. Osteocytes lacking MMP14 exhibit reduced dendritic processes [31], emphasizing MMP14's role in dendritic formation. Despite numerous dendrites in preosteocytes, HIF signaling can diminish MMP14 enzyme capability, suggesting a role in dendritic maintenance.

Osteocytogenesis occurs in a hypoxic environment [8], underscoring the probably function of oxygen sensing and HIF signaling in skeletal homeostasis. Our work demonstrated the important role of oxygen sensing or HIF signaling in regulating osteocytogenesis and skeletal homeostasis, and suggests that impaired LCN networks in conditions like osteopenia or aging may stem from insufficient HIF signaling. Although many hypoxia-mimicking agents have promising effects for osteoporosis and skeletal fractures, we cannot exclude the role of HIF signaling in promoting angiogenesis. Further research is needed to elucidate therapeutic strategies targeting LCN network homeostasis.

However, our study only examined dendrite length and number, limiting insights into polarity and spatial parameters of dendrite formation. Incorporating computer-aided analysis, such as CAM-VT [32–34], could provide a more comprehensive understanding of dendrite formation and the regulatory role of HIF signaling pathways during osteocytogenesis.

In conclusion, our study supports the "actively migration" hypothesis for osteocytogenesis and sheds light on mechanisms underlying impaired LCN networks in VHL-deficient mice. These findings caution against unchecked HIF-1α activation in therapeutics targeting bone diseases, emphasizing the need for moderation in altering the HIF-1α signaling pathway for clinical applications.

4. Materials and methods

4.1. Antibodies

The Catalog No. of antibodies used in this work were listed as following: MMP14 (ab51074), β-actin (ab8226), tubulin (ab7291) and VHL (ab270968) were obtained from Abcam; Cortactin (11381-1-AP) was obtained from ProteinTech Group; HIF-1α (NB100-105) was obtained from Novus Biologicals; pho-ERM (3726) and RhoA (2117) were obtained from Cell Signaling Technology; Texas Red-X conjugated Phalloidin (T7471) and E11 (MA5-16113, clone 8.8.1) were both obtained from Invitrogen.

4.2. Cell culture and treatment

Osteoblast-to-osteocyte transition cell line IDG-SW3 were gifted from L. Bonewald [35]. Cells were proliferated and differentiated under different mediums, with 50 U/ml IFN-γ (#PMC4031, Invitrogen) at 33 °C for proliferation or with 4 mM β-Glycerophosphate (G9422, Sigma) and 50 μg/ml L-ascorbic acid (A4544, Sigma) at 37 °C for differentiation. Cells were seeded on Rat tail type I collagen (A1048301, Gibco) coated plates (0.15 mg/ml collagen in 0.02 M acetic acid coating for 1 h). For 3D extracellular matrix culture system, experiments were performed according to our previous protocol [36].

Hypoxia treatment was performed in a triple-gas incubator (Panosonic, Japan) with an atmosphere containing 1 % O_2 and 5 % CO_2.

4.3. TRITC-crosslinked gelatin degradation assay

TRITC-crosslinked gelatin was prepared similar to previous protocol [15,37]. Briefly, gelatin (G0262, Sigma) was labeled with TRITC (abs42028267, Absin, China) by mixing gelatin solution (5 % in PBS buffer (#10010023, invitrogen)) and TRITC for 1 h. Followed by the reaction solution were dialyzed against double-distilled water to remove the unreacted TRITC molecule. The purified TRITC labeled gelatin were obtained by freeze-drying. Finally, 2.5 % TRITC-labeled gelatin and 2.5 % sucrose (V900116, Sigma) contained PBS was prepared for TRITC-crosslinked gelatin degradation assay.

The coverslips were inverted on a 0.1 ml drop of TRITC-labeled gelatin and crosslinked with 1 % glutaraldehyde (G6257, Sigma) for 5 min at room temperature. After PBS washing, coverslips were quenched with 5 mg/ml sodium borohydride for 3 min, washed three times in PBS, and subjected to cell seeding and IF staining experiment.

4.4. Western blot

Proteins were separated with 10 % SDS–PAGE gels and transferred to nitrocellulose membranes. To reduce nonspecific background, membranes were blocked with 5 % milk in TBS-T buffer. Bands were detected using various antibodies against at 4 °C overnight. The membranes were incubated with peroxidase-conjugated secondary antibodies (1:5000, Jackson) for 1 h at 37 °C before detection using ECL system (EMD Millipore). Images scanned with ImageQuant LAS 4000 mini (GE) were exported as TIFF images in RGB mode.

4.5. Bulk RNA sequencing (RNA-seq)

Osteocytes were harvested similar to the described protocol [38]. Briefly, the outer surfaces of long bones were scraped and digested to remove the periosteum. After cutting off the epiphyses and flushing out the bone marrow, bone fragments contained osteocytes were cut into 1 mm longitude pieces and subjected to tissue grinder in 1 ml TRIzol Reagent at 4 °C. The grinder option is 55 Hz shaking for 1 min every 3 cycles. Then, total RNA was extracted from WT or VHL^{OC} mice using TRIzol Reagent. The poly(A) mRNA isolation was performed using Poly(A) mRNA Magnetic Isolation Module. Sequencing libraries were constructed using the NEBNext® Ultra™ II DNA Library Prep Kit for Illumina and quantified and qualified by Agilent 4200 Bioanalyzer (Agilent Technologies, Palo Alto, CA, USA) and Qubit 4 (Thermo Fisher Scientific Inc.). After sequencing, clean data were analyzed on Illumina DRAGEN Bio-IT Platform (v4.0) with Mus musculus reference genome (mm10) according to the standard RNA-seq analysis flow. TPM value of all the genes were imported to *RStudio* software (planted with *R* version 4.3.3) and different expression genes (DEGs) were analyzed with *EdgeR* (version 4.0.16) package at a threshold of $|Log2FC| > 1$ & PValue <0.01.

4.6. Functional enrichment analysis of DEGs

The DAVID database (https://david.ncifcrf.gov/) was used to identify statistically significant gene ontology (GO) terms that were enriched with DEGs. All results were plotted using the *ggplot2* (version 3.5.0) package.

4.7. Gene set enrichment analysis

The gene sets of the DEGs were sorted and subjected to Gene set enrichment analysis (GSEA) with GSEAPreranked tool in *GSEA* software (version 4.0.0). The HALLMARK gene set and GO_BP gene set was obtained from the *MSigDB* database. The normalized enrichment score (NES) in GSEA was obtained.

4.8. Construction of protein–protein interaction network

The Search Tool for the Retrieval of Interacting Genes/proteins (STRING; https://string-db.org/) database contains both the known and predicted protein interactions, these were used to construct the PPI network. The DEGs was imported into the STRING online platform, and PPI analysis was performed with the default settings and imported into *Cytoscape* software (version 3.9.1). The hub PPI network was screened and visualized using the *MCODE* analysis plugin. Genes from the hub PPI network were treated as hub genes for subsequent analysis.

4.9. Plasmids and siRNA oligo transfection

The pcDNA3.1-HIF-1α-PPN mutant plasmid or VHL and HIF-1α siRNA oligos were both obtained from Shanghai TranSheepBio Biological Technology Co. Ltd. The plasmids or mixed siRNA oligos pool were transfected into cells with Lipofectamine 2000 (Invitrogen) according to the manufacturer's instructions.

For HIF-1α siRNA sequences, siHIF-1α-1 (sense): 5′-GCUGACCAGUUACGAUUGUdTdT-3'; siHIF-1α-2 (sense): 5′-CUGAUAACGUGAACAAAdTdT-3'; siHIF-1α-3 (sense): 5′-GACACAGCCUCGAUAUGAAdTdT-3'.

For VHL siRNA sequences, siVHL-1 (sense): 5′-CCGCAUAUGUAGGGCAUAUdTdT-3'; siVHL-2 (sense): 5′-GUUAACCAAACGGAGCUGUdTdT-3'; siVHL-3 (sense): 5′-CAUUGCCAGUGUAUACCCUdTdT-3'.

4.10. Primary osteoblasts isolation

Three newborn mice (C57BL/6JGpt) were purchased from Charles River (China). The primary osteoblasts were isolated from calvarias of the newborn mice by serial round of digestion with 1.8 mg/ml type I collagenase (17018029, Gibco) [39].

4.11. If staining

IDG-SW3 cells or primary osteoblasts grown on coverslips were fixed with 4 % paraformaldehyde, permeabilized with 0.3 % Triton X-100, washed with PBS and incubated with 2 % BSA containing primary antibodies at 4 °C overnight. The monolayers were then washed with PBS and incubated with appropriate secondary antibodies (Molecular Probes, Invitrogen) in PBS at 37 °C for 1 h. Cells were washed again with PBS, counterstained with DAPI (Beyotime, China) and then used for observation.

4.12. Scanning electron microscope (SEM)

Cells grown on the coverslips were fixed in 2.5 % glutaraldehyde overnight at 4 °C. Cells then washed twice by phosphate buffer, post-fixed in 1.0 % osmium tetroxide in 0.1 M phosphate buffer [pH 7.2] for 2 h at 4 °C, before being washed 3 times with double-distilled water and dehydrated through a graded series of ethanol to 100 %. The surface morphology was observed using a SEM (Hitachi H-7650) at an accelerating voltage of 10 kV.

4.13. Images acquisition

Images were acquired using the Zeiss 800 laser scanning confocal microscopy system on a Zeiss Axio Observer Z1 inverted microscope, equipped with a Plan Apochromat × 63.0, 1.4 numerical aperture oil-immersion, differential interference contrast objective. Scanning was performed using 1024 × 1024 format, 1.58 μs pixel dwell, 16 bit depth, 4 × line average and 1AU (optimal) pinhole. Images were taken on random, but cells with extraordinarily strong or low expression levels were excluded for examination. Lossless fluorescence images obtained from IF were processed in *Fiji* software (version 2.14.0) and exported as TIFF mode files in red/green/blue (RGB) channels. Line profiles were all analyzed within 8-bit format images with *Fiji* software.

4.14. Statistical analysis

The representative data from three independent experiments are present as mean ± S.E.M. Two-tailed *t* tests are utilized for determine significances between two groups. Significance values and N numbers for each data set are shown in each figure legend. All statistical analyses were performed using GraphPad Prism 10.0 software.

Data availability statement

All data needed to evaluate the conclusions in the paper are present in the paper and/or the Supplementary Materials. Data related to this paper may be requested from the authors.

Funding statement

This work was supported by the National Natural Science Foundation of China (82070902, 81700778, 82272556).

CRediT authorship contribution statement

Xiaoyan Li: Investigation, Data curation. **Jian Zhao:** Software, Methodology, Formal analysis, Data curation. **Lei Chen:** Validation, Software, Methodology. **Xinyi Zhou:** Methodology. **Minglong Qiu:** Visualization, Validation. **Lianfu Deng:** Supervision, Funding acquisition, Conceptualization. **Kai Yang:** Writing – review & editing, Writing – original draft, Funding acquisition, Conceptualization. **Yaozeng Xu:** Writing – review & editing, Writing – original draft, Supervision, Conceptualization.

Declaration of competing interest

The authors declare that they have no known competing financial interests or personal relationships that could have appeared to influence the work reported in this paper.

Acknowledgments

We thank Dr. Lynda F Bonewald for gifting IDG-SW3 cell line.

Appendix A. Supplementary data

Supplementary data to this article can be found online at https://doi.org/10.1016/j.heliyon.2024.e32889.

References

[1] S.C. Manolagas, Birth and death of bone cells: basic regulatory mechanisms and implications for the pathogenesis and treatment of osteoporosis, Endocr. Rev. 21 (2000) 115–137, https://doi.org/10.1210/edrv.21.2.0395.

[2] R.L. Jilka, R.S. Weinstein, T. Bellido, A.M. Parfitt, S.C. Manolagas, Osteoblast programmed cell death (apoptosis): modulation by growth factors and cytokines, J. Bone Miner. Res. : the official journal of the American Society for Bone and Mineral Research 13 (1998) 793–802, https://doi.org/10.1359/jbmr.1998.13.5.793.

[3] S.L. Dallas, L.F. Bonewald, Dynamics of the transition from osteoblast to osteocyte, Ann. N. Y. Acad. Sci. 1192 (2010) 437–443, https://doi.org/10.1111/j.1749-6632.2009.05246.x.

[4] T. Bellido, Osteocyte-driven bone remodeling, Calcif. Tissue Int. 94 (2014) 25–34, https://doi.org/10.1007/s00223-013-9774-y.

[5] B. Yu, A. Pacureanu, C. Olivier, P. Cloetens, F. Peyrin, Assessment of the human bone lacuno-canalicular network at the nanoscale and impact of spatial resolution, Sci. Rep. 10 (2020) 4567, https://doi.org/10.1038/s41598-020-61269-8.

[6] L.F. Bonewald, The amazing osteocyte, J. Bone Miner. Res. : the official journal of the American Society for Bone and Mineral Research 26 (2011) 229–238, https://doi.org/10.1002/jbmr.320.

[7] L.M. Tiede-Lewis, S.L. Dallas, Changes in the osteocyte lacunocanalicular network with aging, Bone 122 (2019) 101–113, https://doi.org/10.1016/j.bone.2019.01.025.

[8] A.M. Zahm, M.A. Bucaro, P.S. Ayyaswamy, V. Srinivas, I.M. Shapiro, C.S. Adams, K. Mukundakrishnan, Numerical modeling of oxygen distributions in cortical and cancellous bone: oxygen availability governs osteonal and trabecular dimensions, Am. J. Physiol. Cell Physiol. 299 (2010) C922–C929, https://doi.org/10.1152/ajpcell.00465.2009.

[9] G.L. Zuo, L.F. Zhang, J. Qi, H. Kang, P. Jia, H. Chen, X. Shen, L. Guo, H.B. Zhou, J.S. Wang, Q. Zhou, N.D. Qian, L.F. Deng, Activation of HIFa pathway in mature osteoblasts disrupts the integrity of the osteocyte/canalicular network, PLoS One 10 (2015) e0121266, https://doi.org/10.1371/journal.pone.0121266.

[10] G.L. Semenza, HIF-1 and mechanisms of hypoxia sensing, Curr. Opin. Cell Biol. 13 (2001) 167–171, https://doi.org/10.1016/s0955-0674(00)00194-0.

[11] K. Chen, J. Zhao, M. Qiu, L. Zhang, K. Yang, L. Chang, P. Jia, J. Qi, L. Deng, C. Li, Osteocytic HIF-1alpha pathway manipulates bone micro-structure and remodeling via regulating osteocyte terminal differentiation, Front. Cell Dev. Biol. 9 (2021) 721561, https://doi.org/10.3389/fcell.2021.721561.

[12] B. Fernandez-Munoz, M.M. Yurrita, E. Martin-Villar, P. Carrasco-Ramirez, D. Megias, J. Renart, M. Quintanilla, The transmembrane domain of podoplanin is required for its association with lipid rafts and the induction of epithelial-mesenchymal transition, Int. J. Biochem. Cell Biol. 43 (2011) 886–896, https://doi.org/10.1016/j.biocel.2011.02.010.

[13] C. Merceron, K. Ranganathan, E. Wang, Z. Tata, S. Makkapati, M.P. Khan, L. Mangiavini, A.Q. Yao, L. Castellini, B. Levi, A.J. Giaccia, E. Schipani, Hypoxia-inducible factor 2alpha is a negative regulator of osteoblastogenesis and bone mass accrual, Bone Res 7 (2019) 7, https://doi.org/10.1038/s41413-019-0045-z.

[14] W.Y. Kim, M. Safran, M.R. Buckley, B.L. Ebert, J. Glickman, M. Bosenberg, M. Regan, W.G. Kaelin Jr., Failure to prolyl hydroxylate hypoxia-inducible factor alpha phenocopies VHL inactivation in vivo, The EMBO journal 25 (2006) 4650–4662, https://doi.org/10.1038/sj.emboj.7601300.

[15] E. Martin-Villar, B. Borda-d'Agua, P. Carrasco-Ramirez, J. Renart, M. Parsons, M. Quintanilla, G.E. Jones, Podoplanin mediates ECM degradation by squamous carcinoma cells through control of invadopodia stability, Oncogene 34 (2015) 4531–4544, https://doi.org/10.1038/onc.2014.388.

[16] K. Fujita, Q. Xing, S. Khosla, D.G. Monroe, Mutual enhancement of differentiation of osteoblasts and osteocytes occurs through direct cell-cell contact, J. Cell. Biochem. 115 (2014) 2039–2044, https://doi.org/10.1002/jcb.24880.

[17] H. Suzuki, M.K. Kaneko, Y. Kato, Roles of podoplanin in malignant progression of tumor, Cells 11 (2022), https://doi.org/10.3390/cells11030575.

[18] K. Kurata, T.J. Heino, H. Higaki, H.K. Vaananen, Bone marrow cell differentiation induced by mechanically damaged osteocytes in 3D gel-embedded culture, J. Bone Miner. Res. : the official journal of the American Society for Bone and Mineral Research 21 (2006) 616–625, https://doi.org/10.1359/jbmr.060106.

[19] L.F. Bonewald, The role of the osteocyte in bone and nonbone disease, Endocrinol Metab Clin North Am 46 (2017) 1–18, https://doi.org/10.1016/j.ecl.2016.09.003.

[20] E. Ikpegbu, L. Basta, D.N. Clements, R. Fleming, T.L. Vincent, D.J. Buttle, A.A. Pitsillides, K.A. Staines, C. Farquharson, FGF-2 promotes osteocyte differentiation through increased E11/podoplanin expression, J. Cell. Physiol. (2017), https://doi.org/10.1002/jcp.26345.

[21] K.A. Staines, B. Javaheri, P. Hohenstein, R. Fleming, E. Ikpegbu, E. Unger, M. Hopkinson, D.J. Buttle, A.A. Pitsillides, C. Farquharson, Hypomorphic conditional deletion of E11/Podoplanin reveals a role in osteocyte dendrite elongation, J. Cell. Physiol. 232 (2017) 3006–3019, https://doi.org/10.1002/jcp.25999.

[22] J.L. Astarita, S.E. Acton, S.J. Turley, Podoplanin: emerging functions in development, the immune system, and cancer, Front. Immunol. 3 (2012) 283, https://doi.org/10.3389/fimmu.2012.00283.

[23] E. Martin-Villar, D. Megias, S. Castel, M.M. Yurrita, S. Vilaro, M. Quintanilla, Podoplanin binds ERM proteins to activate RhoA and promote epithelial-mesenchymal transition, J. Cell Sci. 119 (2006) 4541–4553, https://doi.org/10.1242/jcs.03218.

[24] Q. Dang, J. Liu, J. Li, Y. Sun, Podoplanin: a novel regulator of tumor invasion and metastasis, Med. Oncol. 31 (2014) 24, https://doi.org/10.1007/s12032-014-0024-6.

[25] V.V. Artym, Y. Zhang, F. Seillier-Moiseiwitsch, K.M. Yamada, S.C. Mueller, Dynamic interactions of cortactin and membrane type 1 matrix metalloproteinase at invadopodia: defining the stages of invadopodia formation and function, Cancer Res. 66 (2006) 3034–3043, https://doi.org/10.1158/0008-5472.CAN-05-2177.

[26] E.S. Clark, A.S. Whigham, W.G. Yarbrough, A.M. Weaver, Cortactin is an essential regulator of matrix metalloproteinase secretion and extracellular matrix degradation in invadopodia, Cancer Res. 67 (2007) 4227–4235, https://doi.org/10.1158/0008-5472.CAN-06-3928.

[27] K.A. Staines, M. Prideaux, S. Allen, D.J. Buttle, A.A. Pitsillides, C. Farquharson, E11/Podoplanin protein stabilization through inhibition of the proteasome promotes osteocyte differentiation in murine in vitro models, J. Cell. Physiol. 231 (2016) 1392–1404, https://doi.org/10.1002/jcp.25282.

[28] K. Zhang, C. Barragan-Adjemian, L. Ye, S. Kotha, M. Dallas, Y. Lu, S. Zhao, M. Harris, S.E. Harris, J.Q. Feng, L.F. Bonewald, E11/gp38 selective expression in osteocytes: regulation by mechanical strain and role in dendrite elongation, Molecular and cellular biology 26 (2006) 4539–4552, https://doi.org/10.1128/MCB.02120-05.

[29] D.M. Gilkes, L. Xiang, S.J. Lee, P. Chaturvedi, M.E. Hubbi, D. Wirtz, G.L. Semenza, Hypoxia-inducible factors mediate coordinated RhoA-ROCK1 expression and signaling in breast cancer cells, Proc. Natl. Acad. Sci. U.S.A. 111 (2014) E384–E393, https://doi.org/10.1073/pnas.1321510111.

[30] M.A. Karsdal, T.A. Andersen, L. Bonewald, C. Christiansen, Matrix metalloproteinases (MMPs) safeguard osteoblasts from apoptosis during transdifferentiation into osteocytes: MT1-MMP maintains osteocyte viability, DNA Cell Biol. 23 (2004) 155–165, https://doi.org/10.1089/104454904322964751.

[31] K. Holmbeck, P. Bianco, I. Pidoux, S. Inoue, R.C. Billinghurst, W. Wu, K. Chrysovergis, S. Yamada, H. Birkedal-Hansen, A.R. Poole, The metalloproteinase MT1-MMP is required for normal development and maintenance of osteocyte processes in bone, J. Cell Sci. 118 (2005) 147–156, https://doi.org/10.1242/jcs.01581.

[32] M. Li, S. You, W. Liu, H. Sun, Y. Wang, M. Grzegorzek, C. Li, LFD-CD: Peripheral Blood Cells Detection Using a Lightweight Cell Detection Model with Full-Connection and Dropconnect, Springer Nature Switzerland, Cham, 2023, pp. 623–633.

[33] Z. Fan, X. Wu, C. Li, H. Chen, W. Liu, Y. Zheng, J. Chen, X. Li, H. Sun, T. Jiang, M. Grzegorzek, C. Li, CAM-VT: a Weakly supervised cervical cancer nest image identification approach using conjugated attention mechanism and visual transformer, Comput. Biol. Med. 162 (2023) 107070, https://doi.org/10.1016/j.compbiomed.2023.107070.

[34] A. Chen, C. Li, S.J. Zou, M.M. Rahaman, Y.D. Yao, H.Y. Chen, H.C. Yang, P. Zhao, W.M. Hu, W.L. Liu, M. Grzegorzek, SVIA dataset: a new dataset of microscopic videos and images for computer-aided sperm analysis, Biocybern. Biomed. Eng. 42 (2022) 204–214, https://doi.org/10.1016/j.bbe.2021.12.010.
[35] S.M. Woo, J. Rosser, V. Dusevich, I. Kalajzic, L.F. Bonewald, Cell line IDG-SW3 replicates osteoblast-to-late-osteocyte differentiation in vitro and accelerates bone formation in vivo, J. Bone Miner. Res. : the official journal of the American Society for Bone and Mineral Research 26 (2011) 2634–2646, https://doi.org/10.1002/jbmr.465.
[36] K. Chen, H. Chen, L. Deng, K. Yang, J. Qi, IDG-SW3 cell culture in a three-dimensional extracellular matrix, J. Vis. Exp. (2023), https://doi.org/10.3791/64507.
[37] A. Steffen, G. Le Dez, R. Poincloux, C. Recchi, P. Nassoy, K. Rottner, T. Galli, P. Chavrier, MT1-MMP-dependent invasion is regulated by TI-VAMP/VAMP7, Curr. Biol. : CB 18 (2008) 926–931, https://doi.org/10.1016/j.cub.2008.05.044.
[38] L. Zhong, L. Yao, R.J. Tower, Y. Wei, Z. Miao, J. Park, R. Shrestha, L. Wang, W. Yu, N. Holdreith, X. Huang, Y. Zhang, W. Tong, Y. Gong, J. Ahn, K. Susztak, N. Dyment, M. Li, F. Long, C. Chen, P. Seale, L. Qin, Single cell transcriptomics identifies a unique adipose lineage cell population that regulates bone marrow environment, Elife 9 (2020), https://doi.org/10.7554/eLife.54695.
[39] L.F. Zhang, J. Qi, G. Zuo, P. Jia, X. Shen, J. Shao, H. Kang, H. Yang, L. Deng, Osteoblast-secreted factors promote proliferation and osteogenic differentiation of bone marrow stromal cells via VEGF/heme-oxygenase-1 pathway, PLoS One 9 (2014) e99946, https://doi.org/10.1371/journal.pone.0099946.